Nanoscale Evidence Unravels Microalgae Flocculation Mechanism Induced by Chitosan

Irem Demir, Jonas Blockx, Etienne Dague, Pascal Guiraud, Wim Thielemans, Koenraad Muylaert, Cécile Formosa-Dague

Nanoscale evidences unravel microalgae flocculation mechanism induced by chitosan

Irem Demir[1,2ǂ], Jonas Blockx[3,4ǂ], Etienne Dague[2,5], Pascal Guiraud[1,5], Wim Thielemans[3], Koenraad Muylaert[3,4], and Cécile Formosa-Dague[1,5*]

[1]TBI, Université de Toulouse, INSA, INRAE, CNRS, Toulouse, France

[2]LAAS, Université de Toulouse, CNRS, Toulouse, France

[3]Sustainable Materials Lab, Department of Chemical Engineering, KU Leuven, Campus Kulak Kortrijk, Belgium

[4]Laboratory for Aquatic Biology, KU Leuven, Campus Kulak Kortrijk, Belgium

[5]Fédération de recherche FERMAT, CNRS, Toulouse, France

ǂThese two authors equally contributed to the work

Corresponding author: Cécile Formosa-Dague, formosa@insa-toulouse.fr

ABSTRACT

~~In light of climate change, there is a growing interest for sustainable energy~~. Microalgae are a promising resource for biofuel production, although their industrial use is limited by the lack of effective harvesting techniques. Flocculation consists in the aggregation and adhesion of cells into flocs that can be more easily removed from water than individual cells. Although it is an efficient harvesting technique, contamination is a major issue as chemical flocculants are often used. An alternative is to use natural biopolymers flocculants, such as chitosan. Chitosan is a bio-based non-toxic polymer, which has been effectively used to harvest *Chlorella vulgaris* cells at pH lower than its pKa (6.5). While the flocculation mechanism reported relied on electrostatic interactions between chitosan and the negative cell surface, no molecular evidence has yet confirmed this mechanism. In this study, we performed force spectroscopy AFM experiments to probe the interactions between *C. vulgaris* cells and chitosan at the molecular scale to decipher its flocculation mechanism. Our results showed that at pH 6, chitosan interacts with *C. vulgaris* cell wall through biological interactions, rather than electrostatic interactions. These observations were confirmed by comparing the data with cationically modified cellulose nanocrystals, for which the flocculation mechanism, relying on an electrostatic patch mechanism, has already been described for *C. vulgaris.* Further AFM experiments also showed that a different mechanism was at play at higher pH, based on chitosan precipitation. Thus this AFM-based approach highlights the complexity of chitosan-induced flocculation mechanisms for *C. vulgaris.*

KEYWORDS: Atomic force microscopy, Force spectroscopy, Microalgae, Flocculation, Chitosan, Cellulose nano-crystals

These last two decades, the global interest for microalgae has increased, notably because of their oil production capacity that makes them an interesting alternative resource for biofuel production.[1] Indeed, several studies have estimated that microalgae could produce between 40 000 and 90 000 L of biofuel per Ha, depending on the sunlight and the biomass oil content of the species considered.[2–4] This represents up to 200 times more liters than soybean and 25 times more liters than oil palm.[5] Among the wide variety of microalgae species, several have been considered for biofuel production such as *Chlorella vulgaris*. *C. vulgaris* is a unicellular freshwater microalgae species first discovered in 1890 by a Dutch researcher.[6] This species first attracted attention in the 1950s for its nutritional value, as its protein content represents up to 55% of its dry mass[7]. Nowadays, *C. vulgaris* is mainly used for nutraceutical purposes; studies have shown for example that it has immune-modulating and anti-cancer properties[8,9], but has also received interest for biofuel production[4]. Indeed, *C. vulgaris* has the capacity to accumulate important amounts of lipids under certain culture conditions, with a fatty acid profile adapted for biofuel production.[7,10,11]

But presently, the commercialization of microalgae-based biofuels is hindered by the lack of economically competitive harvesting techniques, as this step is generally estimated to represent 20-30% of the total microalgal biomass production cost.[12,13] In the case where the harvesting step is combined with lipid extraction, as needed in biofuel production processes, this cost can increase up to 90%, resulting in a negative energy balance for the production of microalgae-based biofuels at large scale.[14–16] The parameters that make harvesting microalgae such a challenging task are their low concentration in water, their small cell size, their negatively charged surface, and their low density. So far, different harvesting techniques have been proposed, including centrifugation, filtration, flotation, flocculation, and electrical-based processes. A recent review compared and described the advantages and disadvantages of each of these techniques.[13] Among them, flocculation stands out as it is inexpensive, making it an option for large-scale harvesting for a wide

variety of microalgae species.[17] Flocculation consists in the aggregation of cells to facilitate their separation from water by sedimentation or flotation for example. While this technique presents many advantages, a major issue in flocculation is contamination, as it often requires the use of chemical flocculants to induce flocculation, which end up in the harvested biomass, and can interfere with downstream processes or with its final application.[18] In this context, an interesting alternative is to use biopolymers to induce flocculation[19], the most popular in microalgae harvesting being chitosan.

Chitosan is a cationic polyelectrolyte obtained by deacetylation of chitin, an abundant natural polymer. Chitosan presents many advantages compared to traditional inorganic flocculants as it is non-toxic, biodegradable, biocompatible, and renewable.[20,21] Moreover, chitosan does not contaminate the harvested biomass as chitin-like polysaccharides are naturally present in the cell wall of many microalgae species, including *C. vulgaris*, and thus harvested cells can then be directly exploited.[22] Chitosan-induced flocculation has so far been used to harvest successfully both fresh-water and marine microalgae species. For fresh-water species such as *C. vulgaris*, its efficiency is mostly attributed to the amino groups present in chitosan. These groups have a pKa value of about 6.5[23], and thus below this pH these groups are mostly protonated and confer a positive charge to chitosan, which allows supposedly its electrostatic interaction with the negatively charged surface of microalgae cells.[24] As a result, cells are believed to be flocculated through a charge neutralization mechanism.[25–27] In the case of marine microalgae species, mixed results on chitosan efficiency have been reported. Indeed, at the high ionic strengths of marine waters, it is believed that the positives charges of chitosan are shielded, preventing further flocculation through charge neutralization. However some studies reported successful flocculation of certain marine species by chitosan[28–31], which may suggest that chitosan-induced flocculation may rely on different interactions between chitosan and cells than electrostatic interactions. In this view, an interesting paper from 2011 focused on the influence of the cell wall carbohydrate composition of *C. vulgaris* on the efficiency of chitosan-induced flocculation.[32] The results obtained in this study show that a higher polysaccharide

content (including neutral sugars, uronic acids and amino sugars) in the cell wall is associated with a better efficiency of flocculation with chitosan at high pH (8.5), suggesting that non-electrostatic absorption of chitosan on cells may be more important than electrostatic neutralization in *C. vulgaris*. However, in all the reported cases of flocculation of *C. vulgaris* using chitosan as a flocculant, no molecular evidences has been provided, so that the mechanism(s) underlying the flocculation remains unclear.

In this study, we investigated the interactions between chitosan and *C. vulgaris* cells using an advanced technique: atomic force microscopy (AFM). AFM, first developed in 1986[33], is a highly sensitive force machine able to record forces as small as 20 pN, making it possible to gain insights into the molecular interactions between single living cells and their environment. Our team recently used AFM to understand the flocculation mechanism involved in the cases of three different microalgae species, demonstrating the interest of using this technology to answer such questions.[34–36] Thanks to AFM force spectroscopy experiments, we show for the first time that at pH 6 below its pKa, chitosan interacts with *C. vulgaris* cell wall through non-electrostatic interactions, *i. e.* through specific interactions between chitosan and polymers at the surface of cells that are being unfolded upon retraction. These observations were confirmed by comparing the data obtained with cationically modified cellulose nanocrystals (CNCs), for which the flocculation mechanism, relying on an electrostatic patch mechanisms, has been suggested in a previous study from our team on *C. vulgaris*.[37] Further AFM experiments, including force spectroscopy but also roughness analysis, however showed that at higher pH, the mechanism at play is different, as chitosan is not able to interact with cells at such high pH. Thus our AFM-based approach allows in this study to highlight the complexity of chitosan-induced flocculation in the case of *C. vulgaris*, and enabled us to identify, at pH 6, a new flocculation mechanism based on the biological binding of chitosan with the cell wall of cells. Given the wide use of chitosan in microalgae harvesting processes, these new data provide important information to optimize microalgae-based biofuel production.

RESULTS AND DISCUSSION

Macroscopic observations show that chitosan does not interact electrostatically with cells

In a previous work where we evaluated the efficiency of cationically-modified CNCs to flocculate *C. vulgaris* cells, we showed that the number of positive charges present on the CNCs was directly correlated with the flocculation efficiency.[37] Indeed, CNCs bearing more positive charges allowed more efficient flocculation compared to CNCs with less positive charges. This was explained by the fact that positive CNCs interact with cells through electrostatic interactions, and thus the more positive charges present, the more interactions can occur with cells, resulting in a higher flocculation efficiency. Based on the literature, this situation should be similar for chitosan at a pH of 6, so below the pKa value of the amine groups of chitosan. To test this hypothesis, we performed flocculation experiments using different chitosan molecules with different degrees of deacetylation (DD), thus bearing more or less positive charges. The DD of each chitosan was determined using conductometric titration and established to be of 77.5 ± 0.8%, 80.5 ± 1.4% and 85.2 ± 0.2% (see Figure S1 and Table S1). The dynamic viscosity of the chitosan stock solutions (5 g/L in 0.04 M HCl) was measured under different shear stress (see Table S2). Chitosan in solution acts as a non-newtonian liquid: increasing shear stress reduces the dynamic viscosity. The results obtained for the flocculation experiments are presented in figure 1a. They show that surprisingly, the flocculation efficiency is similar for all chitosans tested, with a maximum efficiency reached for a dose of 10 mg/L, thus showing that there is no influence of the DD of chitosan, and thus of its number of positive charges on the flocculation of cells. This in line with the work of Chen *et al.*, who also showed that the DD of chitosan had indeed a limited impact on the flocculation of bentonite.[38] Moreover, this study also showed that the molecular weight of chitosan had a dominant influence on the flocculation efficiency, with high molecular weights allowing to reach higher flocculation efficiencies. In our case, the MW of the chitosan that was used is of 345.2 kDa, thus high, which explains perhaps the high efficiencies reached in our flocculation experiments (> 95%). To verify this observation, we compared the flocculation efficiencies with a pH of 8 where chitosan does not present positive

charges. In this case, if the flocculation efficiency of chitosan is based on electrostatic interactions, then no flocculation should be observed at this higher pH environment. However, the results obtained, presented in Figure 1b, show that a maximum flocculation efficiency can be reached for the same chitosan dose both at pH 6 and 8. While this efficiency drops at higher doses for a pH of 6, it remains maximum for doses up to 80 mg/L for a pH of 8. This result can be correlated to previous data obtained in our team for the marine species *Nannochloropsis occulata* where it was shown that chitosan was efficient even when used at higher pH conditions.[31] It was showed that at higher pH, the uncharged chitosan precipitates causing the flocculation of the cells through a sweeping mechanism where cells are mechanically trapped in the massive structure of the precipitate[39], instead of charge neutralization as it is supposed to be the case at pH 6. Overall the flocculation results presented here seem not to be in accordance with the literature, and comfort the idea, previously raised in 2011 in the case of *C. vulgaris*[32], that the interactions between cells and chitosan may not rely on electrostatic interactions.

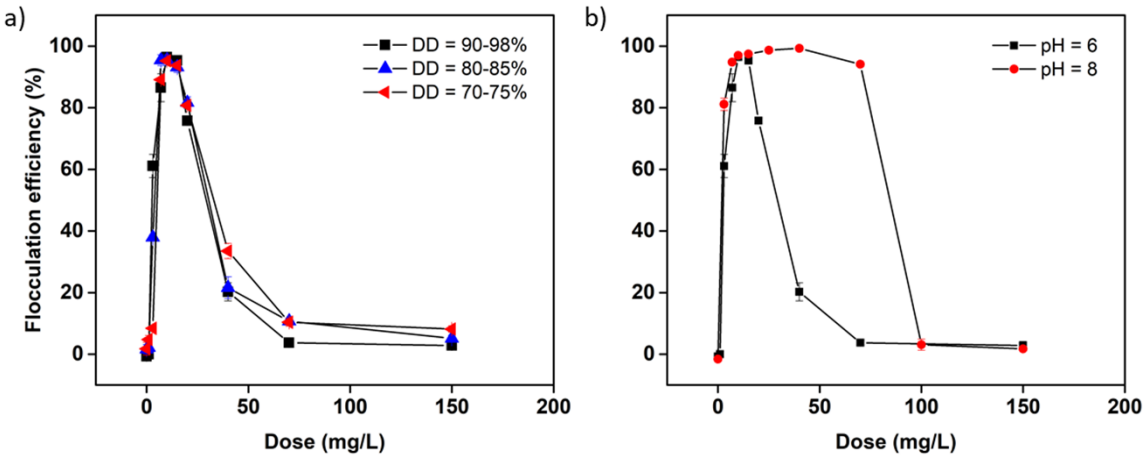

Figure 1: Flocculation experiments of *C. vulgaris* with chitosan. Flocculation efficiency of a) different chitosan molecules with different deacetylation degree (DD) at pH 6 and b) chitosan molecules with DD = 77.5 ± 0.8% at pH 6 and 8.

To understand this phenomena further, we performed an optical microscopy assay with cells incubated with CNCs and chitosan used at concentrations for which the best flocculation efficiencies were obtained (10 mg/mL for chitosan and 100 mg/L for CNCs[37]). For chitosan, we chose to work

with the chitosan with a degree of deacetylation of 77.5 ± 0.8% (4.2 mmol charges/g). Three types of CNCs were used in this study: unmodified CNCs, CNCs modified with pyridinium grafts (CNC-PYR, DS = 0.20, 0.92 mmol charges/g) and CNCs modified with methylimidazolium grafts (CNC-MIM, DS = 0.23, 0.99 mmol charges/g). The used CNCs were fully characterized in a previous study by the authors.[37] Both CNC-PYR and CNC-MIM have quaternary ammonium groups which carry a permanent positive charge independent of pH, unlike chitosan, for which the charge carried by its primary amines are only charged after protonation at low pH.[37,40] The results are presented in Figure 2. When CNCs were used, CNCs particles can directly be observed on the images (indicated by arrows): in the case of unmodified CNCs (Figure 2a), no cells are attached to the particles, while for CNC-PYR and CNC-MIM, cells aggregated around the particles could be observed (Figure 2b and c). This is then coherent with the patch mechanism already described for *C. vulgaris* in our previous work where cells interact electrostatically with CNC particles. Thus, in the case of unmodified CNCs that do not have positive charges, no interactions with cells could be observed. However for chitosan, the situation is different: at pH 6, small aggregates of cells were observed, with smaller size than the CNC aggregates (Figure 2e), suggesting that chitosan does interact with cells, but that perhaps the nature of the bond is different, not as strong as in the case of CNCs. At pH 8, cells do not seem to be aggregated (Figure 2f). If we follow the hypothesis formulated in our previous work on *N. occulata*[31], then this results could be explained by the fact that at higher pH, the flocculation mechanism is based on sweeping, and thus there are no direct interactions between chitosan and cells. This is also in line with what was already demonstrated on another microalgae species, *Dunaliella salina*; when sweeping mechanism is involved, there are no interactions between the flocculant and the cells.[35] Thus, at this stage, our macroscopic analysis seems to show that in contrast to the literature, chitosan-induced flocculation in *C. vulgaris* may not rely on electrostatic interactions, even at pH 6 where chitosan is positively charged. However, what is then the mechanism involved?

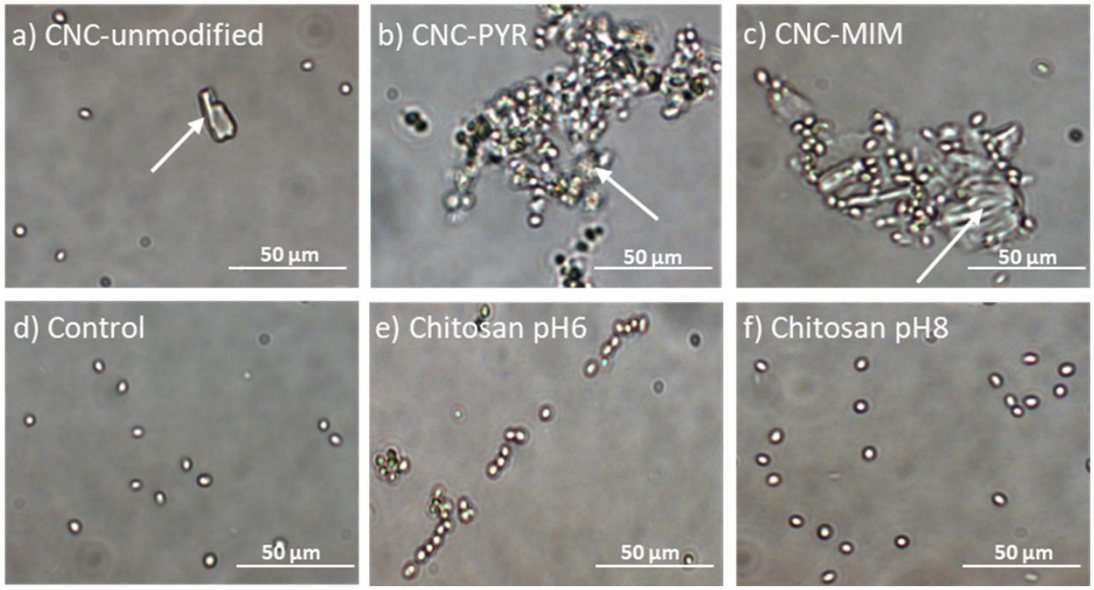

Figure 2. Optical imaging of *C. vulgaris* flocculation. Optical image of *C. vulgaris* cells after resuspension in PBS containing a) 100 mg/L of CNC-unmodified at pH 8, b) 100 mg/L of CNC-PYR at pH 8, c) 100 mg/L of CNC-MIM at pH 8, d) nothing at pH 6, e) 10 mg/L of chitosan at pH 6, and f) 10 mg/L of chitosan at pH 8. The arrows in a), b) and c) indicate the CNC particles.

AFM nanoscale scale experiments reveal the role of biological interactions between cells and chitosan during flocculation

To answer this question, we used atomic force microscopy (AFM) in order to directly probe the interactions between the flocculants and cells and to get a better insight into the flocculation mechanisms involved in each case. We first performed force spectroscopy experiments to probe the interactions between CNCs and single *C. vulgaris* cells. For that, a first method (method 1 described in the Methods section, Figure S2a) has consisted in using tips directly modified with CNCs (Figure S3) to probe the interactions with cells immobilized on a positive glass surface at a pH of 8. In the case of

CNCs, the charge present on the particles is not dependent on the pH because the modified CNCs carry a quaternary ammonium group that is permanently positively charged. But because this first method was difficult to implement for modified CNCs, as the forces recorded between the CNCs particles and cells were stronger than the electrostatic forces between the cells and the surface on which they were immobilized, only a small number of cells could be probed. Indeed, during force spectroscopy, the cells would detach from the surface to adhere to the CNC particle on the probe, therefore making the measurements impossible. To overcome this challenge, we also recorded data using FluidFM technology (method 2 in the Methods section, Figure S2b). In this case, single cells were aspirated at the aperture of microfluidic probes by exerting a negative pressure inside the cantilever microchannel. This negative pressure was sufficient to keep the cells attached to the cantilever, and thus more measurements could be performed. The data presented in Figure 3 combines data obtained with these two methods for modified CNCs (details of these data can be found in Table S3); in the case of unmodified CNCs, only the first method was used. In this figure, the adhesion forces, rupture distances and representative force curves recorded in PBS buffer are presented. The adhesion force corresponds to the strongest adhesion event in each force curve, while the rupture length is the distance of the last adhesion event recorded. The percentage of adhesion indicated corresponds to the percentage of force curves presenting retract adhesions. In each case, the results presented correspond to the interactions recorded with 10 cells coming from at least 2 independent cultures. In the case of unmodified CNCs (Figure 3a and b), and in line with our previous work, no interactions with cells can be observed, as retract force curves show no retract peaks. In the case of CNC-PYR (Figure 3c and d), a single retract peak happening at the contact point can be observed, with in this case an average force of 1.2 ± 0.7 nN (n = 9801 force curves). This force signature is typical of non-specific interactions, most likely reflecting electrostatic interactions between the negative surface of the cells and the positive surface of PYR-modified CNCs.[34] Similar force curves could be obtained for CNCs-MIM (Figure 3e and f), however, in this case the average adhesion force recorded was of 3.5 ± 2.6 nN (n = 8845 force curves), so almost 3 times higher than

for CNCs-MIM. The adhesion force difference between CNC-MIM and PYR is significant at a p-value of 0.001 (unpaired t-test). This is an interesting point; indeed, CNC-MIM have a higher number of positive charges compared to CNC-PYR, and our results indicate that this difference influence the adhesion force recorded. Thus the more positive charges on the CNCs are present, the stronger the electrostatic bond with the cell's surface is. However, the difference in DS between both cationic CNCs is small (CNCs-PYR, DS = 0.20 and CNCs-MIM, DS = 0.23), not fully explaining the big differences in adhesion forces. An explanation for these differences might reside in the chemical structure of the cationic grafts on the CNCs. In the CNC-PYR sample, the cationic charge is distributed over a 6-membered ring, while only over a 5-membered ring in the CNC-MIM sample, causing different charge densities at the atomic level. Moreover methylimidazolium has two nitrogen atoms in its ring structure, while pyridinium only contains one; this could also contribute to the difference recorded in the adhesion forces. Regarding the rupture distance recorded, they were in average of 18.6 ± 26.1 nm for CNC-PYR, and of 18.6 ± 22.1 nm for CNC-MIM, indicating that no molecules were pulled away from the surface of the cells. Thus, these results confirmed that the interactions between cationic CNCs and cells are non-specific and electrostatic. Hence, this molecular data confirms that in the case of CNCs-induced flocculation a charge neutralization mechanism is involved, and it explains why better flocculation efficiencies are obtained using CNCs bearing a higher number of positive charges. To further prove this point, and exclude possible contributions of other types of interactions between CNCs and cells, additional experiments were carried out to measure the interactions between beads bearing COOH functionalities, thus negatively charged at a pH of 8, and CNCs immobilized on mica surfaces. These beads have a similar size to the cells, and thus are here used as artificial non-living analogues of microalgae cells bearing only negative charges and no surface polymers. The results (Figure S4) show the same tendency, *i. e*. single peak retract force curves and lower adhesion values obtained with CNCs-PYR (5.3 ± 1.4 nN, n = 800 force curves obtained with 2 different beads), compared to CNCs-MIM (49.6 ± 10.6 nN, n = 800 force curves obtained with 2 different beads). In this case, the adhesion values are higher than the ones obtained with cells; this

can be explained by the fact that the beads were more negatively charged than cells. Indeed, zeta potential measurements have shown that at a pH of 8, cells have a surface potential of –21.9 mV, whereas the zeta potential of beads is of –43.2 mV.

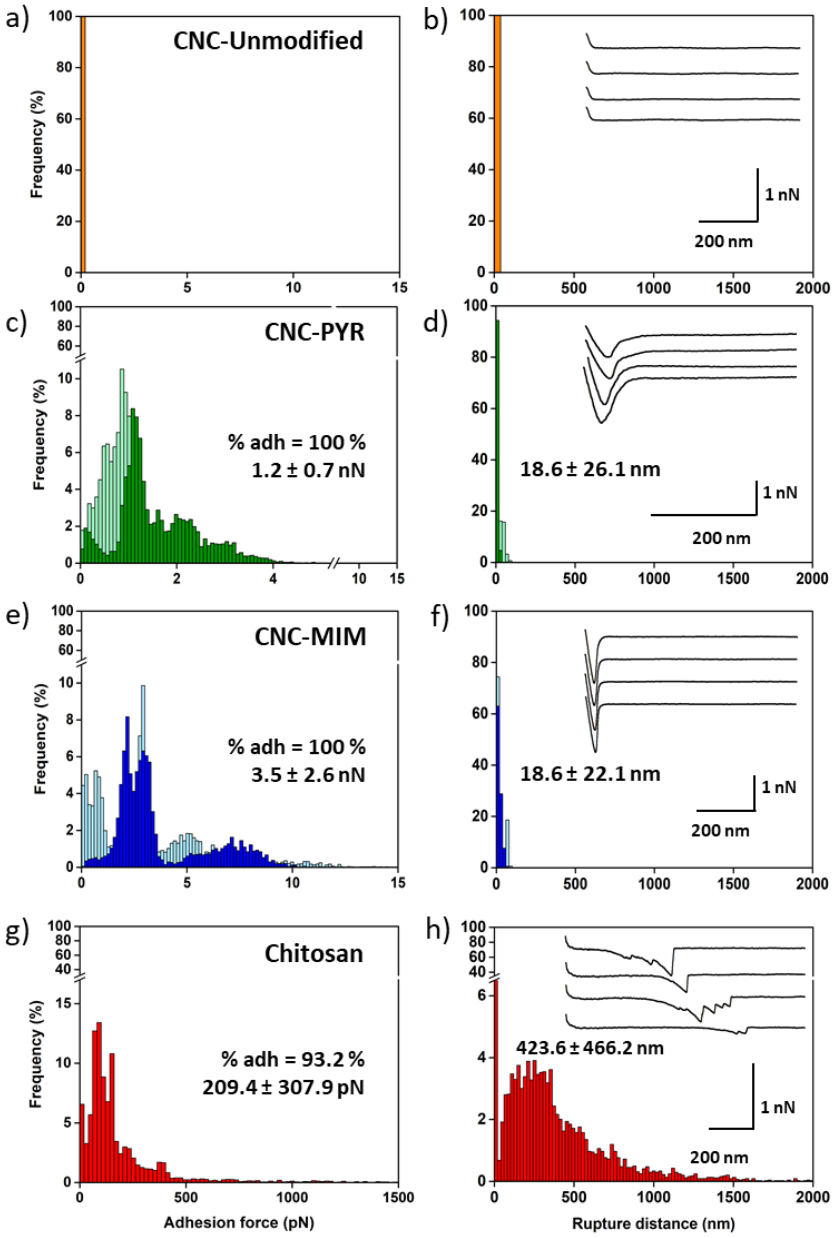

Figure 3. Interactions between CNCs or chitosan and single *C. vulgaris* cells. a) Adhesion force histogram between *C. vulgaris* cells and CNCs-unmodified at pH 8 and b) corresponding rupture distance histogram. c) Adhesion force histogram between *C. vulgaris* cells and CNCs-MIM at pH 8 and d) corresponding rupture distance histogram. The light green distributions correspond to values obtained with method 1 and the dark green distributions correspond to values obtained with method 2. e) Adhesion force histogram between *C. vulgaris* cells and CNCs-MIM at pH 8 and f) corresponding rupture distance histogram. The light blue distributions correspond to values obtained with method 1 and the dark blue distributions correspond to values obtained with method 2. g) Adhesion force histogram between *C. vulgaris* cells and chitosan spin-coated on a glass slide at pH 6 and h)

corresponding rupture distance histogram. Insets in b), d), f) and h) show representative force curves obtained. Data were recorded using a set-point of 0.25 nN.

However, the interesting result from these force spectroscopy analysis concerns chitosan (Figure 3g and h). In this case, the interactions between a single living *C. vulgaris* cell immobilized at the edge of a tipless cantilever[41], and a chitosan-functionalized surface by spin-coating[42,43] were probed at a pH of 6 (method 3 in the Methods section, Figure S2c). In this case, retraction force profiles showed multiple binding events with an average adhesion force of 209.4 ± 307.9 pN (n = 5698 force curves), thus much lower than the forces recorded for cationic CNCs. In contrast, the average rupture length for chitosan was 423.3 ± 466.2 nm, whereas in the case of cell interactions with CNCs it was close to zero. Note that the large standard deviations come from the wide distributions of the values visible on the histograms, caused by the heterogeneity inherent to living cells. The extended ruptures, the low adhesion forces recorded, as well as the lack of defined force patterns are consistent with the stretching of long molecules from the cell wall of cells.[44–46] Given the difference in the force signatures obtained, our results suggest that in the case of chitosan, even when positively charged, no electrostatic interactions are involved in the bonding with cells, or at least if electrostatic interactions are involved they are not predominant in the interactions and are masked by the biological interactions. This inherently implies that chitosan is able to interact specifically with polymers present at the surface of cells that are then unfolded upon retraction in our force spectroscopy experiments, resulting in the long rupture distances observed. Taking into account the work of Cheng and coworkers, who showed that the carbohydrate composition of the cell wall of *C. vulgaris* has a direct influence on the efficiency of flocculation obtained with chitosan[32], we may suggest that chitosan is able to specifically interact with these polysaccharides. Moreover, similar force patterns were already observed for microalgae by Higgins and coworkers who extended mucilage (composed of polysaccharides) from the cell wall of *Craspedostauros australis*, a marine diatom, and of *Pinnularia viridis*, a freshwater diatom[47]. This further supports that the unfolding observed in our case may be due to the unfolding of polysaccharides from the *C. vulgaris* cell wall. For the moment, such specific structural interactions between chitosan and polysaccharides, not

dependent on electrostatic interactions, have been described only in a few cases, for example with cellulose[48] or with alginate,[49] for which interactions with chitosan have been observed at high or low pH, where either the polysaccharides or the chitosan are uncharged. Moreover, previous studies have also reported the possible interaction between chitosan and glycopolymers in the case of microorganism flocculation: for example Barany *et al.* showed that *Escherichia coli* flocculation by chitosan relied on chitosan absorption to polymers from the cells, rather than on electrostatic factors.[50] Thus, at this stage, the data obtained indicate that chitosan flocculation at pH 6 in the case of *C. vulgaris* does not occur through electrostatic interactions, but rather through biological interactions, meaning that chitosan interacts with biomolecules at the cell surface that are then unfolded from the cell surface. These biomolecules might be polysaccharides present at the surface of the cells. More questions can now be raised: can further data prove this? Is this mechanism also at play at pH 8?

Chitosan induced-flocculation of *C. vulgaris* at higher pH does not occur through the same mechanism

To further investigate the flocculation mechanism of chitosan, we decided to compare the interactions between chitosan and cells at pH 6 and 8 at varying applied forces. When the applied force is increased during force spectroscopy experiments, because the chitosan layers are deformable (Ym of 15.6 ± 30.5 kPa at pH 6, n=1554 force curves, and of 19.2 ± 23.2 kPa at pH 8, n=1349 force curves, values extracted from force curves at an indentation segment of 100 nm, data not showed), the contact area between the cells and the chitosan surface increases as well. This increase should lead to higher adhesion forces as more molecules from the cell wall are able to interact with the chitosan surface; rupture lengths will also provide useful information on the nature of the molecules unfolded. The results of these experiments are presented in Figure 4, they were obtained in the case of a set point of 0.25 nN with 10 different cells, and in the case of higher set points with 4 different cells coming from at least 2 independent cultures (details of the data can be

found in Table S3, S4 and S5). In each case, the differences between the adhesion forces recorded at pH 6 and pH 8, for the different set-points, are significantly different at a p-value of 0.001 (unpaired t-test). At pH 6, we can observe that the more the applied force was increased, the more the average adhesion force increased, from 209.4 ± 307.9 pN at an applied force of 0.25 nN (Figure 4a, n = 5698 force curves), to 296.6 ± 327.1 pN at 1 nN (Figure 4c, n = 2050 force curves) and 444.9 ± 398.9 pN at 2 nN (Figure 4e, n = 2050 force curves), thus two times higher. As for the rupture distances, they also increase with the applied force, from in average 423.6 ± 466.2 nm at 0.25 nN (Figure 4b) up to 679.7 ± 523.3 nm at 2 nN (Figure 4f). This thus indicates that as the contact surface area increases between the cell and the chitosan surface, the more molecules, probably polysaccharides, from the cell wall involved in the interactions with chitosan were extended, resulting in higher adhesion forces and rupture distances. When these experiments were performed at a pH of 8, a similar trend was observed, with an increase in both the maximum adhesion force and rupture length when the applied force is higher. However, an interesting point to note in this case is the difference in values between the measurements performed at pH 6 and pH 8. Indeed, in the case of pH 8, the average adhesion force recorded was 193.1 ± 182.8 pN at an applied force of 2 nN (Figure 4k, n = 2050 force curves), thus almost equivalent to the adhesion force recorded at pH 6 for the smallest applied force (0.25 nN). Regarding rupture lengths, although the average distances recorded were similar at a high force applied, their difference is important at a low applied force (423.6 ± 466.2 nm at pH 6 and 320.9 ± 362.5 nm at pH 8). The differences in these values are surprising as one would expect that if the interaction mechanism is indeed based on biological interactions, the same molecules would unfold from the cell surface irrespective of the pH, resulting in similar unfoldings with similar rupture distances. These results thus seem to indicate that it is not the case.

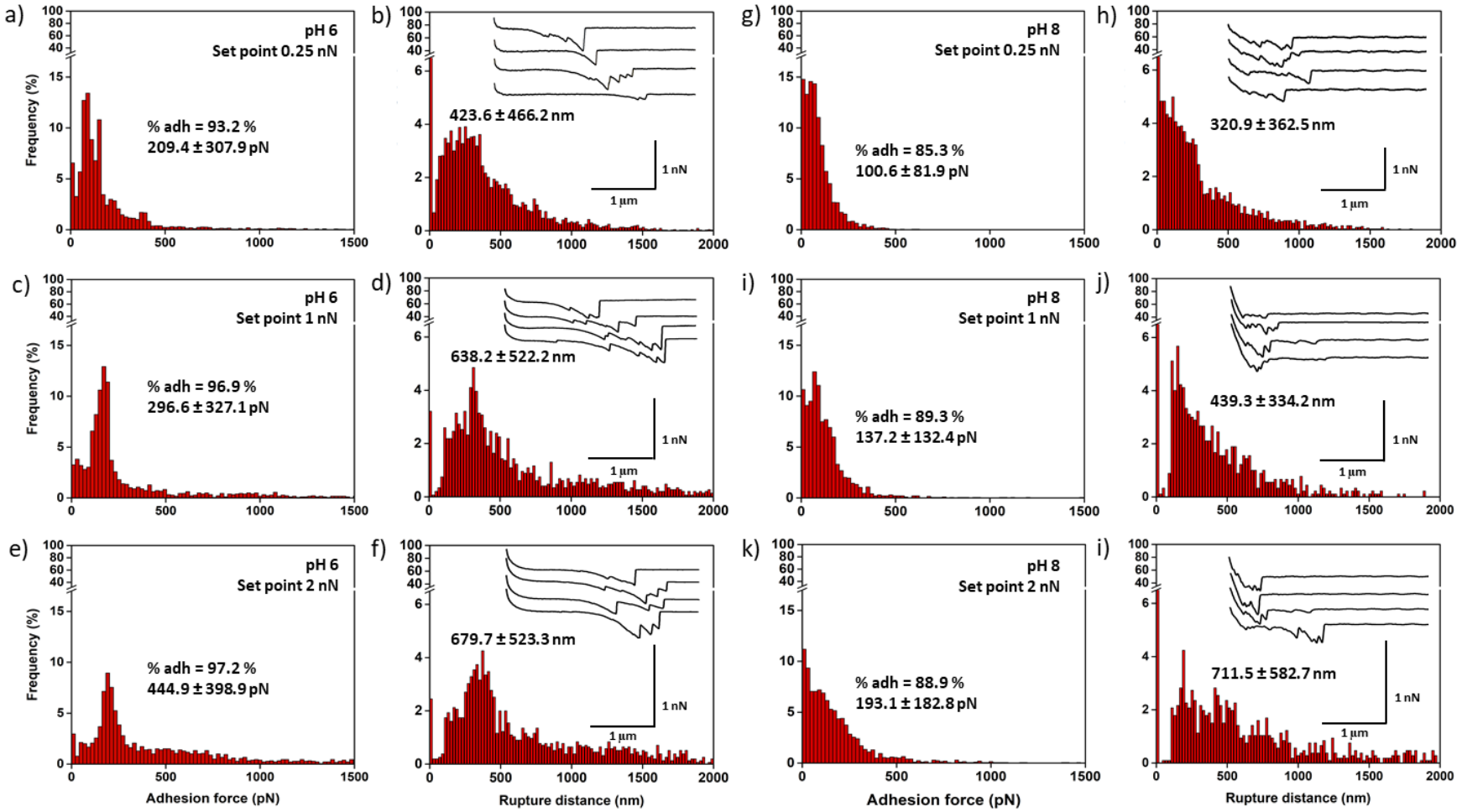

Figure 4. Interaction between chitosan and single *C. vulgaris* cells at pH 6 and 8 at varying applied forces. a) Adhesion force histogram and b) corresponding rupture distance histogram betweens a *C. vulgaris* cell-functionalized cantilever and chitosan spin-coated on a glass slide at pH 6 using a set-point of 0.25 nN, c) and d) using a set-point of 1 nN, e) and f) using a set-point of 2 nN. g) Adhesion force histogram and h) rupture distance histogram between a *C. vulgaris* cell-functionalized cantilever and chitosan spin-coated on a glass slide at pH 8 using a set-point of 0.25 nN, i) and j) using a set-point of 1 nN, k) and l) using a set-point of 2 nN. Insets in b), d), f), h), j) and l) show representative force curves obtained.

To understand this behavior, we performed experiments with negatively charged beads, and probed the interactions with chitosan surfaces at pH 6 and 8. The results are presented in Figure 5. At pH 6, few interactions were recorded between the beads and the chitosan surface (2.8 % of the force curves), as most retract force curves present no retract peaks (Figure 5a and b). This thus proves our first hypothesis that chitosan interactions with cells do not rely dominantly on electrostatic interactions but on biological interactions. Indeed, COOH beads enables us to mimic the cell surface by bearing negative charges, but have the advantage to exclude the molecules that are present on the cell walls. In this case, it is clear that the biological polymers that are present on the microalgal cell surface are essential for the interaction of chitosan with the cell, and that the charge of chitosan is not dominant in the interaction with cells in our experimental conditions. Moreover, as for experiments where the interactions between cells and chitosan were probed at pH 6 (Figure 4), no electrostatic interactions were recorded. This further indicates that these interactions, either do not take place or are smaller than the limit of detection of AFM (20 pN), and thus cannot be captured. This is an interesting point because at pH 6 chitosan is positively charged, and should in theory interact with negatively charged surfaces; thus perhaps these interactions are too weak to be detected. The poor strength of electrostatic interactions between positively charged chitosan at low pH and negative surfaces has already been described in other research fields. For example, chitosan has been used to bind with negatively charged drugs in order to form drug loaded chitosan nano- and microparticles.[51] However it is showed in several studies that the release of the drugs from chitosan particles is rapid, indicating that the binding properties of chitosan through electrostatic interactions may be poor.[51]

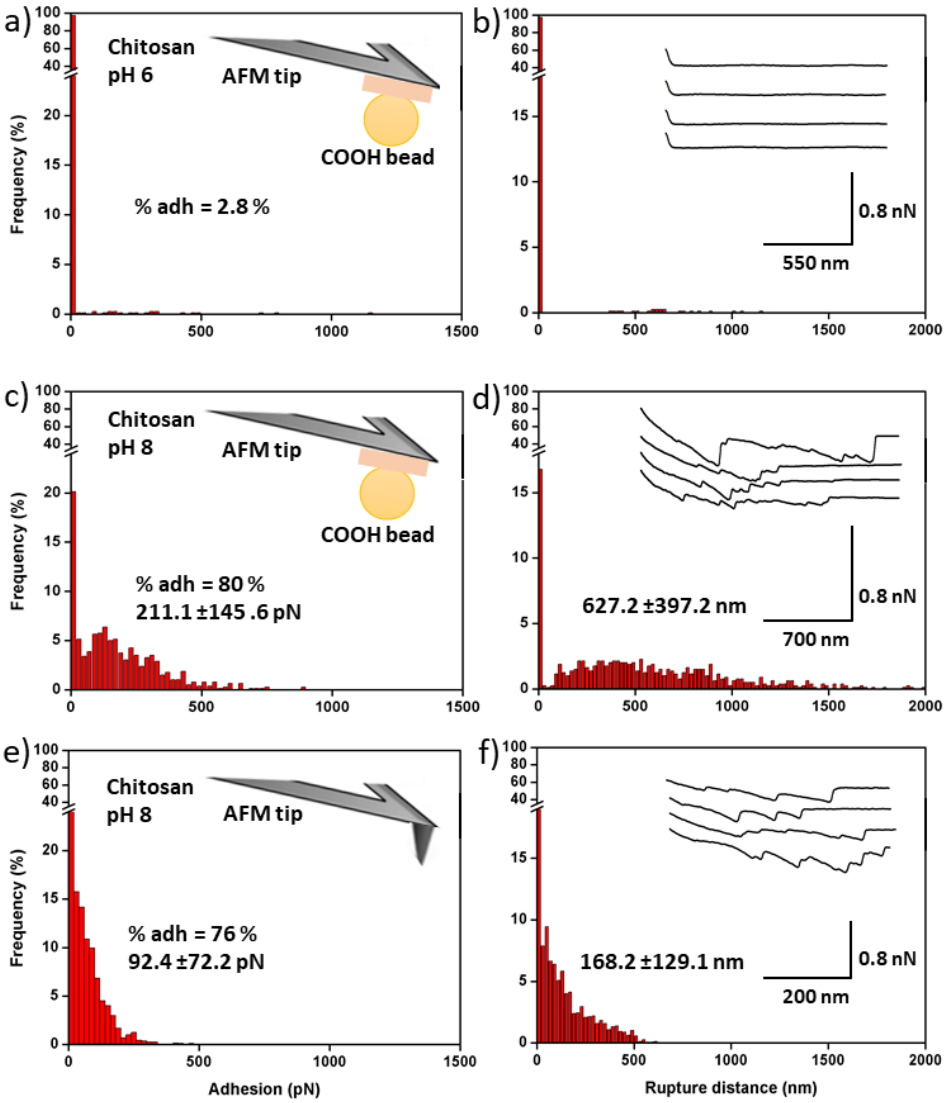

Figure 5. Interaction between bare tips and negative beads-functionalized cantilevers with chitosan surfaces. a) Adhesion force histogram between a COOH bead-functionalized cantilever and chitosan spin-coated on a glass slide at pH 6 and b) corresponding rupture distance histogram. c) Adhesion force histogram between a COOH bead-functionalized cantilever and chitosan spin-coated on a glass slide at pH 8 and d) corresponding rupture distance histogram. e) Adhesion force histogram between a bare AFM tip chitosan spin-coated on a glass slide at pH 8 and f) corresponding rupture distance histogram. Insets in b) d) and f) show representative force curves obtained. Data were recorded using a set-point of 0.25 nN.

When the same experiments are performed at a pH of 8 (Figure 5c and d), force curves show multiple peaks that have a similar profile to the ones obtained using cells instead of beads, with average adhesion forces and rupture lengths recorded values of 211.1 ± 145.6 pN and 627.2 ± 397.2 nm (n = 800 force curves, with 2 different beads), respectively. Using bare tips instead of beads (Figure 5e and f), the same unfolding events were recorded, with similar adhesion and rupture

400 distances values as in the case of cells. This result is unexpected: indeed, the bare tips used, as for
401 the beads, carried no polymers, *i.e.* the multipeaks observed on the force curves must correspond to
402 the unfolding of chitosan picked up directly from the surface upon retraction by the tips or the
403 beads. This indicates that at this pH, the structure of chitosan must be different than at pH 6 where
404 bare tips do not allow the unfolding of chitosan. Moreover, this gives the explanation for the results
405 obtained using living cells at pH 8 (Figure 4g-l): in this case also, the chitosan must be unfolded from
406 the surface which explains why the adhesion forces and rupture lengths values obtained are different
407 from those obtained at pH 6. Given the fact that the same chitosan unfoldings were obtained with
408 cells, negative beads or bare tips, we can thus conclude that at pH 8 there is no biological nor
409 electrostatic interaction between the cells and chitosan, in agreement with the optical images
410 obtained (Figure 2e) where no cell aggregation could be visualized. The fact that higher adhesions
411 and rupture lengths values are recorded with beads compared to cells or bare AFM tips is explained
412 by the fact that the surface contact with beads is larger (6-7 µm of diameter compared to 3-4 µm of
413 diameter for cells), thus allowing the AFM tip to pull more chitosan from the surface. The
414 flocculation mechanism of cells at pH 8 is thus based on a different mechanism than at pH 6; our
415 hypothesis is that at this pH, the chitosan precipitates and flocculates the cells by sweeping, as we
416 have demonstrated in our previous study.[31] We now need to verify this hypothesis.
417
418 **Sweeping mechanism is involved in the flocculation of *C. vulgaris* at pH 8**
419 The previous results have demonstrated that cells do not interact through biological or
420 electrostatic interactions with chitosan at pH 8. However, the question is now to understand if this is
421 due to changes in the cell wall properties of the cells, to changes in the chitosan structure, or to
422 both? It has been shown previously with the marine species *Phaeodactylum tricornutum* that the cell
423 wall rigidity changed with pH, which impacted on the deformability of the cells and thus on their
424 interactions with their environment.[34] Moreover, AFM studies on microorganisms have shown that
425 under some conditions, the architecture and network of molecules at the surface of cells can change

426 depending on the external conditions, which thus impacts on the availability of molecules to interact
427 with their environment.[45] To verify these two points in our study, we performed nanomechanical
428 analysis of the cell wall of cells as well as surface roughness analysis. These results are presented in
429 Figure 6. To obtain quantitative information on the nanomechanical properties of the cells, we
430 determined the Young modulus (Ym) of the microalgae cells trough nanoindentation measurements,
431 in PBS at pH 6 and pH 8 (Figure 6a and b). In this type of measurements, the cantilever, for which
432 mechanical properties are known, is pressed against the cells at a given force. This enables us to
433 extract the Ym of the cell wall, a parameter that reflects its resistance to compression (the higher the
434 Young modulus value, the more rigid the cell wall). Nanoindentation measurements, which give
435 access to force *vs* distance curves, were performed on areas of 500 nm × 500 nm on top of cells, on 8
436 cells coming from at least 2 independent cultures. Ym values were then obtained first by converting
437 the force curves obtained into force *vs* indentation curves, shown in Figure 6a, and then by fitting
438 them with a theoretical model, in our case, the Hertz model[52] (black empty circles on the curves in
439 Figure 6a). The results show that the indentation curves obtained on cells at pH 6 and 8 are different;
440 indeed, the AFM probe is able to indent deeper into cells at pH 6 than at pH 8, meaning that
441 increasing the pH also increases the rigidity of the cell wall. Quantitative analysis of the Ym extracted
442 from thousands of these curves on 8 cells in each case confirmed this finding, and showed that at pH
443 6, cells have an average Ym of 232.9 ± 175.6 kPa (n = 8192 force curves), whereas cells at pH 8 have a
444 Ym of 750.2 ± 589.0 kPa (n = 8182 curves, differences are significant at a p-value of 0.001, unpaired t-
445 test, details can be found in table S6). While the nanomechanical properties of *C. vulgaris* have never
446 been determined using AFM before, these values are in the range of Ym values obtained on other
447 microorganisms such as yeasts, that have a cell wall composition comparable to microalgae.[53]
448 Moreover, this increase in the rigidity, due to the increase of pH, has already been shown in the case
449 of *P. tricornutum*.[34] Hence, increasing the pH changes the nanomechanical properties of the cell wall
450 and thus its architecture, perhaps explaining in part the fact that cells are not able to interact with
451 chitosan at pH 8. Indeed, it could mean that the molecules involved in the interaction with chitosan

452 are not available anymore for interaction, or that their conformation at elevated pH prevents the
453 interaction with chitosan. Regarding the cell wall roughness, this parameter was directly extracted
454 from contact images of 500 nm × 500 nm obtained on top of 8 cells coming from at least 2
455 independent cultures. The results obtained (Figure 6c-f) show that the surface morphology is slightly
456 modified by the increase in pH, as shown by the vertical deflection images recorded on top of the
457 cells in Figure 6c and d. Cross-sections taken along the white lines in Figure 6c and d show this
458 difference, as the profile of this cross-section at pH 8 presents larger motives. The quantitative
459 analysis of the roughness measured on several cells showed that at pH 6, cells have an average
460 roughness of 0.9 ± 0.5 nm while it increased to 1.7 ± 0.9 nm at pH 8. While this difference is
461 significant, it remains low and indicates that at pH 8, more molecules protrude from the surface of
462 the cell, which might mask the molecules involved in the interaction with chitosan, or perhaps might
463 indicate that these molecules are coiled and not able to interact anymore.[45] Overall this biophysical
464 analysis of the cell wall of *C. vulgaris* indicates that a pH increase from 6 to 8 clearly affects its rigidity
465 and its roughness. These changes, as discussed, may explain why cells do not interact with chitosan
466 anymore at pH 8.
467
468
469
470
471
472
473
474
475
476
477

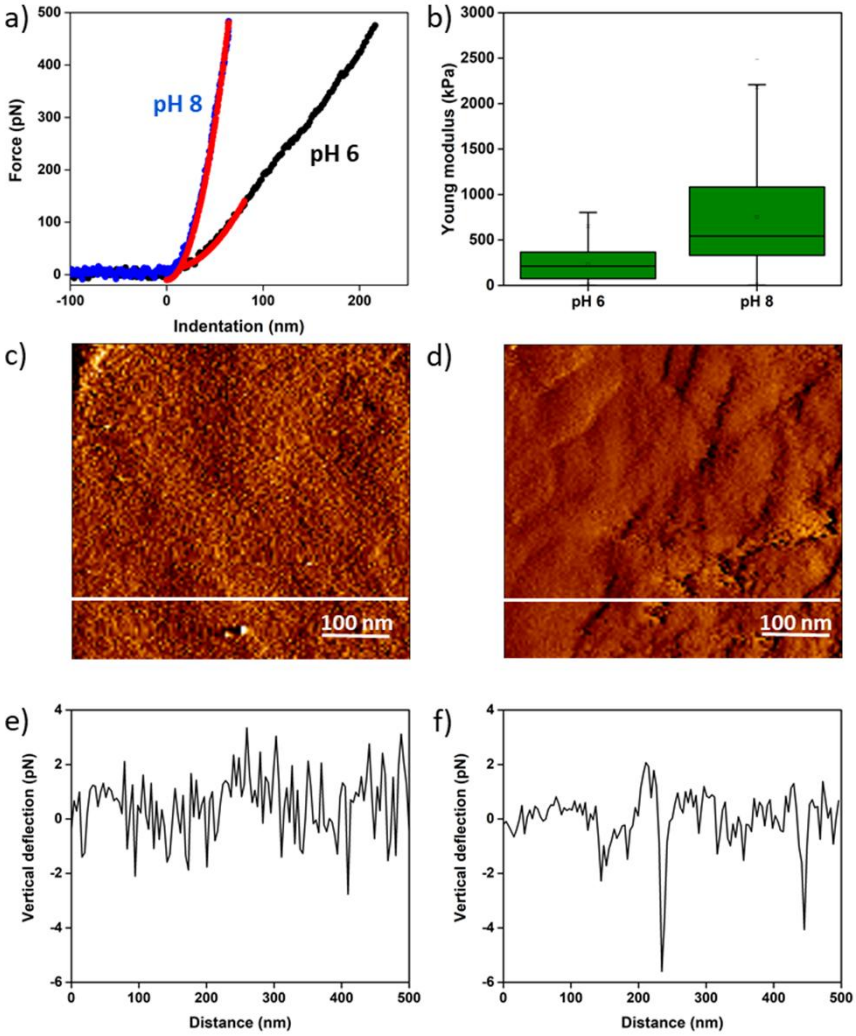

Figure 6. Nanomechanics and cell wall roughness of the *C. vulgaris* cell wall. a) Indentation curves (blue and black lines) fitted with the Hertz model at 80 nm of indentation (red lines) recorded on top of *C. vulgaris cells* at pH 6 and 8. b) Boxplot of the Young's modulus values measured on top of *C. vulgaris* cells at pH 6 and 8. c) Vertical deflection AFM image of an area (500 × 500 nm) of the cell surface at pH 6 and d) vertical deflection AFM image of an area (500 × 500 nm) of the cell surface at pH 8. e) Cross-section taken along the white line in c) and f) cross-section taken along the white line in d).

To determine if this lack of interactions is also due to the chitosan itself, we also performed roughness measurement on the chitosan functionalized surfaces used in all the experiments. The results, presented in Figure 7, showed an average roughness of chitosan of 0.6 ± 0.1 nm at a pH of 6, which increased dramatically, to 13 ± 5 nm at a pH of 8. This result indicates that the pH has an important effect on the structure of the chitosan, which, precipitates and gets detached from the

surface. This detachment from the surface creates aggregates of chitosan, as it can be seen on the height image recorded (Figure 7b), which leads to an important roughness. This explains why chitosan can be pulled out from the surface in force spectroscopy experiments, whatever the probe used (cell, negatively charged bead, or bare AFM tip). This precipitation might lead to a decrease of its specific surface available for interaction, which can also be a rational explanation to the fact that cells do not interact with chitosan at pH 8. Thus, from these experiments, we can conclude that the fact that chitosan does not interact with the cell wall of *C. vulgaris* at pH 8 results from the combination of changes associated directly with the structure of the cell wall with changes in the structure of chitosan itself caused by its precipitation.

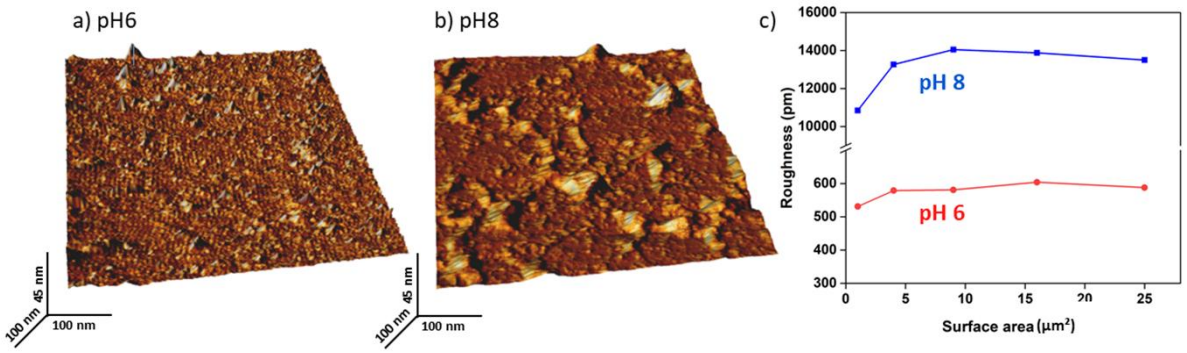

Figure 7. Characterization of chitosan surfaces at two different pH. a) 3D AFM height image of chitosan surface at pH 6. b) 3D AFM height image of chitosan surface at pH 8. c) Quantification of chitosan surface roughness at pH 6 and 8.

CONCLUSION

Chitosan, given its many advantages, has been widely used as a flocculant to efficiently harvest diverse species of microalgae. Since understanding the flocculation mechanisms is key to control them and use them in larger-scale processes, the case of chitosan has generated a lot of debate in the scientific community. Indeed, while for freshwater species that grow at pH below 6.5, chitosan-induced flocculation is believed to rely on a charge neutralization mechanism, some studies also show it becomes more efficient at higher pH, while in marine waters were the salts present screen the charges of chitosan, chitosan can still flocculate microalgae. It is therefore of great importance to provide new data, using original techniques, to finally shed light on the flocculation

515 mechanism at play. For that we have chosen the freshwater green species, *C. vulgaris*, and studied at
516 the nanoscale its interactions with chitosan using atomic force microscopy. Our results demonstrate
517 that depending on the pH, the interaction mechanism is different, which reveals the complexity of
518 chitosan flocculation. Indeed, preliminary macroscopic observations suggest that the charge of
519 chitosan is not involved in the interaction with cells, as different degrees of deacetylation result in
520 the same flocculation efficiency at pH 6. At increased pH, for the same degree of deacetylation, the
521 flocculation behavior is different as high doses of chitosan still allow an efficient separation, which is
522 not the case at pH 6. Based on these observations, our force spectroscopy experiments show that at
523 pH 6, chitosan interacts in a specific way with most probably polysaccharides present on the surface
524 of cells, and that the chitosan charge is not significantly involved in these interactions. This was
525 confirmed by comparing these data with those obtained for cationically modified CNCs, for which a
526 previous study has demonstrated the contribution of only of charge neutralization in the flocculation
527 mechanism.[37] However, such biological interactions between chitosan and the surface of cells could
528 not be detected at pH 8. Indeed, biophysical analysis of the cell wall of *C. vulgaris* cells, as well as
529 roughness analysis of the chitosan used in this study suggest that at this pH, both the architecture of
530 the cell wall and the structure of chitosan are modified, resulting in an absence of interactions with
531 the cells. Based on a previous work published last year where we had found that a sweeping
532 mechanism is involved in the chitosan-induced flocculation of *N. occulata* at high pH, we thus suggest
533 that this mechanism is also at play for the flocculation of *C. vulgaris* at high pH. These different
534 mechanisms of flocculation are depicted in Figure 8. This study thus represents an original
535 contribution to the field of microalgae harvesting as molecular-scale data allow in this case to
536 understand the flocculation mechanisms and to show the important influence of the culture medium
537 pH on these mechanisms. Therefore, this work brings important information that will help in
538 implementing chitosan-induced flocculation to harvest microalgae at large-scale. Further work is now
539 needed to identify the polymers from the cell surface that interact specifically with chitosan at pH 6.
540 Because a large amount of microalgae species share the same surface characteristics, in particular

the composition, this knowledge would make it then be possible to perform efficient chitosan flocculation with a wide range of microalgae species.

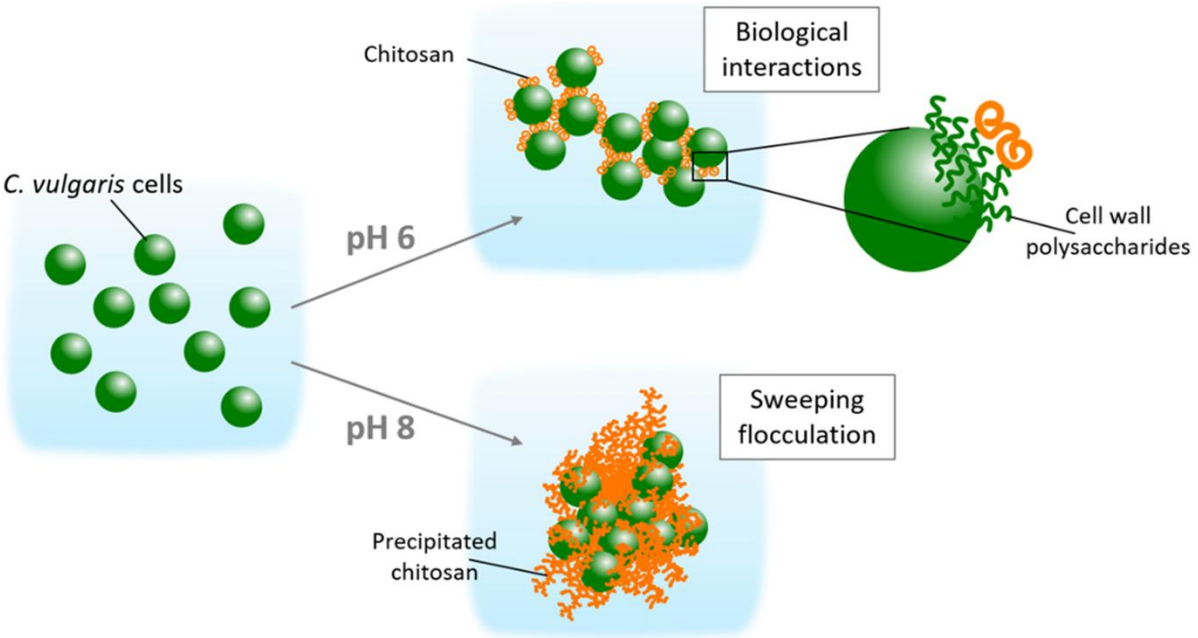

Figure 8. Schematic representation of the flocculation mechanisms induced by chitosan at pH 6 and 8 for *C. vulgaris.*

METHODS

Microalgae cultivation. The green freshwater microalgae *Chlorella vulgaris* strain CCAP 211/11B (Culture Collection of Algae and Protozoa) was cultivated in sterile conditions in Wright's cryptophyte (WC) medium prepared in deionized water, adjusted to a pH of 7.8.[54] Cells were cultivated at 20°C, under agitation (120 rpm), in 1L Erlenmeyer (300 mL of culture) flasks. The incubator was equipped with white neon light tubes providing illumination of approximately 40 µmol photons m^{-2} s^{-1} with a photoperiod of 18h light: 6h dark. All experiments were carried out with exponential phase batch cultures (day 7).

Cationically-modified cellulose nanocrystals (CNCs) synthesis. N-Benzylmethylimidazolium Grafted CNCs ([Br][BnIm]-g-CNCs, referred in the text as CNCs-MIM) and Benzylpyridinium Grafted CNCs

([Br][BnPy]-g-CNCs, referred in the text as CNCs-PYR), were synthesized and characterized in a previous study and described in Blockx *et al.*[37] For the CNCs-MIM, the sample with a degree of substitution (DS) of 0.23 was used, whereas for the CNCs-PYR, the sample with a DS of 0.20 was used.

Chitosan. Three different types of chitosan were used in this study. Commercial chitosan was purchased from Sigma Aldrich (from shrimp, practical grade, ≥75% degree of deacetilation (DD)). In an earlier study it was determined that this chitosan has a M_n and M_w of 151.3 and 345.2 kDa respectively, and a polydispersity of 2.28[31]. This chitosan was used throughout the paper for the flocculation experiments and all AFM experiments. For flocculation experiments, two chitosan samples with different DD (labelled as 70-75% and 80-85%) were prepared from shrimp shells and kindly provided by Nha trang University, Vietnam. Chitosan stock solutions were produced by dissolving 5 g/L of the three types of chitosan in 0.04 M of HCl, while stirring (1000 rpm) at ambient conditions for 2 hours. A more exact degree of deacetylation was determined for the three chitosan samples via conductometric titrations (Metrohm 856 Conductivity Module and 801 Stirrer with TiamoTM software). For that, 2 mL stock solution was diluted 50 fold in MiliQ water and titrated with 5.75 mM NaOH under constant stirring. The results are shown in supplementary Figure S1 and Table S1. The DD was determined from the volume of NaOH required to neutralize the chitosan (plateau area of the curves), where each chitosan sample was measured three times. The DD of the commercial Sigma Aldrich chitosan is of 77.5 ± 0.8%, and for the chitosan samples provided by the Nha trang University of 80.5 ± 1.4% and 85.2 ± 0.2%. The dynamic viscosity of the three chitosan samples was measured on a AR-G2 rheometer (TA Instruments) equipped with a steel double wall couette cell. The experiment consisted of four steps. Step 1: 60 s at a shear rate of 100.0 /s to allow the sample to set in the sample holder; Step 2: 180 s at a shear rate of 1.0 /s; Step 3: 180 s at a shear rate of 10.0 /s; and Step 3: 180 s at a shear rate of 100.0 /s. All experiments were carried out at 25 °C and 1 datapoint was collected per second. All samples were measured in triplicate. Data analysis was performed with TA Instrument Trios Version 3.3.1.4364. The results are showed in Supplementary Table S2.

585 **Flocculation experiments.** Flocculation of *C. vulgaris* was performed using standardized jar tests
586 experiments. The microalgae suspension was adjusted to a pH of 6 and the initial optical density ($OD_{i,}$
587 $_{750\ nm}$) was set at 0.7 (corresponding to 0.28 g/L). 50 mL tests samples were taken and intensively
588 stirred at 550 rpm to mix the suspension. Different concentrations of chitosan were then added (0, 1,
589 3, 7, 10, 15, 20, 40, 70, 150 mg/L) from the 5 g/L stock solutions and the suspensions were stirred at
590 200 rpm for 20 min to induce flocculation. The suspensions were subsequently decanted in falcon
591 tubes and allowed to settle for 30 min before measuring the optical density after settling (OD_f) of the
592 supernatant (at approximately 3 cm below the surface). The flocculation efficiency (η_a) was
593 calculated according to the following equation 1. For experiments at pH 8, the microalgae suspension
594 was adjusted to a pH of 8 priori to flocculation experiments and the chitosan concentrations used
595 were of 0, 3, 7, 10, 15, 25, 40, 70, 100, 150 mg/L.

$$\eta_a = \frac{OD_i - OD_f}{OD_i} \quad (1)$$

596

597 **Optical imaging experiments.** Flocculation was directly observed after resuspension of the cells in
598 Phosphate Buffer Saline (PBS) at a pH of 6 or 8 containing chitosan at a concentration of 10 mg/L or
599 CNCs-PYR or CNCs-MIM, both at a concentration of 100 mg/L. Flocculation levels were observed
600 using an Axio Observer Z1 microscope (Zeiss, Germany) at a magnification of 50x.
601 **Zeta potential experiments.** The global electrical properties of *C. vulgaris* cell surface as well as of
602 negative beads (COOH functionalized polystyrene beads diameter of 6.83 µm, Spherotech, USA) were
603 assessed by measuring the electrophoretic mobility with an automated laser zetameter (Zetasizer
604 NanoZS, Malvern Instruments). To this end, microalgae were harvested by centrifugation (3000 rpm,
605 3 min), washed two times in PBS at a pH of 6 or 8, and resuspended in the same solution at a final
606 concentration of 1.5×10^6 cell/mL. In the case of beads, they were first centrifuged (3 min, 13000
607 rpm) and washed two time in deionized water. For each condition, analysis was performed in
608 triplicate.

AFM cantilever functionalization. All AFM cantilever functionalizations were performed using a Nanowizard III AFM (Bruker, USA), with triangular tipless NP-O10 probes (Bruker, USA, nominal spring constant of 0.06 N/m and of 0.2 N/m).

Functionalization with CNCs**:** Colloidal probes were functionalized with cationic CNC particles. Colloidal probes were obtained by attaching a single silica microsphere (5 µm of diameter, Bangs Laboratories) with a thin layer of UV-curable glue (NOA 63, Norland Edmund Optics). These colloidal probes were then put under UV-light for 10 min to allow the glue to cure. They were further dipped into a thin layer of UV-curable glue, then into a thin layer CNCs particles deposited on a glass slide. Functionalized cantilevers were then put under UV-light for 10 min to allow the glue to cure and further characterized using scanning electron microscopy (Figure S3). The spring constant of the colloidal probe was determined after attachment of the CNC particles using the thermal noise method.[55]

Functionalization with single *C. vulgaris* cells: AFM cantilevers were also functionalized with single *C. vulgaris* cells grown during 7 days in the conditions described previously. For that, cantilevers were first activated using oxygen plasma (3 min, 0.5 mbar) and then incubated in a 0.2% polyethylenimine solution (PEI, Sigma-Aldrich) overnight. The AFM cantilevers were then rinsed in PBS at a pH of 6 or 8, brought into contact with an isolated cell and retracted to attach it. Proper attachment of the cell on the colloidal probe was checked using optical microscopy. The spring constant of the AFM cantilever was determined prior to cell immobilization using the thermal noise method.[55]

Functionalization with negatively charged beads: AFM cantilevers were functionalized using COOH polystyrene beads (negatively charged at pH 6 and 8, diameter of 6.83 µm, Spherotech, USA). Beads were first centrifuged (3 min, 13000 rpm) and washed two time in deionized water. A drop from this solution was then deposited on a glass slide and allowed to dry at 37°C during 2 hours. Cantilevers were first dipped into a thin layer of UV-curable glue (NOA 63, Norland Edmund Optics), and then brought into contact a single isolated bead on the glass slide and retracted to attach it. Functionalized cantilevers were then put under UV-light for 10 min to allow the glue to cure; proper

attachment of the COOH bead on the colloidal probe was checked using optical microscopy. The spring constant of the COOH probe was determined after attachment of the COOH bead using the thermal noise method.[55]

Force spectroscopy experiments. Force spectroscopy experiments were conducted either by functionalizing the cantilever with CNCs and probing the interactions with immobilized cells on a surface (method 1), using FluidFM technology to aspirate a single *C. vulgaris* cell at the aperture of a microfluidic AFM probe to probe interactions with cationic CNCs functionalized on a surface (method 2), or by functionalizing the AFM cantilever with a single *C. vulgaris* cells and probing the interactions with chitosan immobilized on a surface (method 3). In each case, experiments were performed in PBS at a pH of 6 or 8, using a NanoWizard III AFM (Bruker, USA). These 3 methods are also depicted in Figure S2.

Method 1: This method was used to probe the interactions between CNCs or negatively charged beads, and single *C. vulgaris* cells. In this case, CNCs (unmodified, PYR and MIM) or negatively charged beads functionalized cantilevers were directly used to probe the interactions with *C. vulgaris* cells immobilized on polyethylenimine (PEI Sigma P3143) coated glass slides prepared as previously described[56]. For that, cells were first harvested by centrifugation (3000 rpm, 3 min) and washed two times in PBS at pH 6 or 8. Freshly oxygen activated glass slides were covered by a 0.2% PEI solution in deionized water and left for incubation overnight. Then the glass slides were rinsed with deionized water and dried under nitrogen. A total of 1 mL of the cell suspension was then deposited on the PEI slides, allowed to stand for 30 min at room temperature, and rinsed with PBS at pH 6 or 8.

Method 2: This method was also used to probe the interactions between CNCs and single *C. vulgaris* cells. As the forces recorded between CNCs and cells were stronger that the electrostatic forces between PEI coated glass-slides and cells, this method was alternatively used to complete the data sets. In this case, FluidFM technology was used (Cytosurge AG, Switzerland): this system connects the AFM to a pressure pump unit and a pressure controller through a microfluidic tubing system. Micropipette probes with an aperture of 4 µm (spring constant of 0.3 N/m) were used (Cytosurge AG,

Switzerland). First, PBS at a pH 8 was filled in the probe reservoir and was pressed through the cantilever by applying an overpressure (100 mBar). The probe was then immersed in PBS and calibrated using the thermal noise method prior to measurement. A single *C. vulgaris* cell was then picked up from the surface of the Petri dish by approaching the FluidFM probe and applying a negative pressure (−80 mBar). The transfer of the cell on the probe was verified by optical microscopy. The cell probe was then used to probe the interactions with CNCs-functionalized mica surfaces. For that, CNCs solutions at a concentration of 5 g/L were first sonicated for at least for 5 min, then deposited on mica surfaces and left for incubation overnight. After that the mica surfaces were rinsed using PBS at pH 8 and taped at the bottom of the Petri dish used for the AFM experiment.

Method 3: This method was used to probe the interactions between chitosan and single *C. vulgaris* cells. In this case, AFM cantilevers functionalized with a single *C. vulgaris* cells were used to probe the interactions with chitosan-functionalized surfaces, in PBS pH 6 or 8. Chitosan was functionalized at the surface of glass-slide using spin-coating method, according to procedures described in [42,43]. Briefly, 50 mg of chitosan was first dissolved in 10 mL of deionized water containing 30-50 µL of hydrochloric acid (HCl). This solution was then deposited on a clean glass slide and spin-coated at 1000 rpm for 3 min. The glass slides were then dried in an incubator at 50°C overnight, before use.

Roughness analyses. Roughness analyses were performed on cells immobilized on PEI-coated glass slides and on chitosan-functionalized glass slides. In both cases, images were recorded in PBS at pH 6 or 8 using contact mode on a Nanowizard III AFM (Bruker, USA), with MSCT cantilevers (Bruker, nominal spring constant of 0.01 N/m). Images were recorded using an applied force of < 0.5 nN. The cantilevers spring constants were determined by the thermal noise method.[55]

Nanomechanical analysis. For nanoindentation experiments, the applied force was comprised between 0.5 and 2 nN depending on the condition with MSCT cantilevers (Bruker, nominal spring constant of 0.01 N/m). Young's moduli were then calculated from 80 nm indentation curves using the Hertz model[52] in which the force F, indentation (δ) and Young's modulus (Ym) follow equation 2,

where α is the tip opening angle (17.5°), and υ the Poisson ratio (arbitrarily assumed to be 0.5). The cantilevers spring constants were determined by the thermal noise method.[55]

$$F = \frac{2 \times Ym \times \tan \alpha}{\pi \times (1 - \upsilon^2) \times \delta^2} \quad (2)$$

Scanning electron microscopy imaging of AFM cantilevers. AFM cantilevers functionalized or not with CNCs or chitosan were first carbonated and then imaged using a Jeol 6400 electron microscope (Jeol, Tokyo, Japan) equipped with an EDS Bruker SDD detector, at an acceleration voltage of 20kV.

ACKNOWLEDGEMENTS

C. F.-D. is a researcher at CNRS. C. F.-D. acknowledges financial support for this work from the Agence Nationale de la Recherche, JCJC project FLOTALG (ANR-18-CE43-0001-01). J. B., W. T. and K. M. acknowledge financial support for this work from Research Foundation Flanders (grant *G.0608.16N*) and from the EU Interreg France-Wallonie-Vlaanderen program through the ALPO project. W. T. further acknowledges the Provincie West-Vlaanderen for his Chair in Advance Materials, Research Foundation Flanders for his Odysseus fellowship (grant G.0C60.13N), and the European Union's European Fund for Regional Development, Flanders Innovation & Entrepreneurship and the Province of West-Flanders for financial support in the Accelerate^3 project (Interreg Vlaanderen-Nederland program). The authors would like to thank Prof. Dries Vandamme for his contribution in the flocculation experiments.

SUPPORTING INFORMATION

- **Supplementary Table S1.** Conductometric titration results
- **Supplementary Table S2.** Dynamic viscosity at different shear rates (1.0 1/s 10.0 1/s and 100.0 1/s).
- **Supplementary Table S3.** Adhesion force values recorded between single *C. vulgaris* cells and CNCs/chitosan coated surfaces.

- **Supplementary Table S4.** Adhesion force values and percentage of adhesions recorded between single *C. vulgaris* cells and chitosan coated surface at pH 6 with increasing set point (applied force during approach).
- **Supplementary Table S5.** Adhesion force values and percentage of adhesions recorded between single *C. vulgaris* cells and chitosan coated surface at pH 8 with increasing set point (applied force during approach).
- **Supplementary Table S6.** Young's modulus values recorded on *C. vulgaris* cells at pH 6 and pH 8. Values were calculated from 80 nm indentation curves using the Hertz model.
- **Supplementary Figure S1.** Conductometric titration curve of chitosan with DD = 77.5 ± 0.8%, titrated with 5.75 mM NaOH. The replicas and chitosan samples provided by the Nha Trang University have similar results and were not shown.
- **Supplementary Figure S2. Schematic representation of the three force spectroscopy methods used.** a) CNCs (unmodified, PYR and MIM) or negatively charged beads functionalized cantilevers are used to probe the interactions with cells immobilized on polyethylenimine coated glass slides. b) A single *C. vulgaris* cell aspirated at the aperture of a FluidFM probe (4 µm) are used to probe the interactions with CNCs-functionalized mica surfaces. c) AFM cantilevers functionalized with a single *C. vulgaris* cells are used to probe the interactions with chitosan-functionalized surfaces.
- **Supplementary Figure S3.** Scanning electron microscopy imaging of AFM cantilevers. a) AFM cantilever with a single silica bead attached b) AFM cantilever with a silica bead functionalized with an unmodified CNC particle c) AFM cantilever with a silica bead functionalized with a CNC-MIM particle and d) AFM cantilever with a silica bead functionalized with a CNC-PYR particle.
- **Supplementary Figure S4.** Interactions between negative beads and CNC surfaces. a) Adhesion force histogram between a COOH bead-functionalized cantilever and CNC-PYR immobilized on mica at pH 8, b) corresponding rupture distance histogram c) Adhesion force histogram between a COOH bead-functionalized cantilever and CNC-MIM at pH 8 d) corresponding rupture distance

histogram. Insets in b) and d) show representative force curves obtained. Data were recorded using a set-point of 0.25 nN.

AUTHOR İNFORMATİON

Corresponding author: Cécile Formosa-Dague, formosa@insa-toulouse.fr

Toulouse Biotechnology Institute, INSA de Toulouse, 135 avenue de Rangeuil, 31077 Toulouse Cedex 4, France

AUTHOR CONTRİBUTİONS

The manuscript was written through contributions of all authors. All authors have given approval to the final version of the manuscript. ǂ I. D. and J. B. contributed equally to the work.

REFERENCES

(1) Pragya, N.; Pandey, K. K.; Sahoo, P. K. A Review on Harvesting, Oil Extraction and Biofuels Production Technologies from Microalgae. *Renewable and Sustainable Energy Reviews* **2013**, *24*, 159–171. https://doi.org/10.1016/j.rser.2013.03.034.

(2) Algae Bloom Again. *Nature* **2007**, *447* (7144), 520–521. https://doi.org/10.1038/447520a.

(3) Wijffels, R. H.; Barbosa, M. J. An Outlook on Microalgal Biofuels. *Science* **2010**, *329* (5993), 796–799. https://doi.org/10.1126/science.1189003.

(4) Mallick, N.; Mandal, S.; Singh, A. K.; Bishai, M.; Dash, A. Green Microalga Chlorella Vulgaris as a Potential Feedstock for Biodiesel. *Journal of Chemical Technology & Biotechnology* **2012**, *87* (1), 137–145. https://doi.org/10.1002/jctb.2694.

(5) Ziolkowska, J. R. Prospective Technologies, Feedstocks and Market Innovations for Ethanol and Biodiesel Production in the US. *Biotechnology Reports* **2014**, *4*, 94–98. https://doi.org/10.1016/j.btre.2014.09.001.

(6) Beijerinck, M. W. I. Kulturversuche Mit Zoochlorellen, Lichenengonidien Und Anderen Niederen Algen. *Botanische Zeitung* **1890**, *48*, 729.

(7) Safi, C.; Zebib, B.; Merah, O.; Pontalier, P.-Y.; Vaca-Garcia, C. Morphology, Composition, Production, Processing and Applications of Chlorella Vulgaris: A Review. *Renewable and Sustainable Energy Reviews* **2014**, *35*, 265–278. https://doi.org/10.1016/j.rser.2014.04.007.

(8) Morimoto, T.; Nagatsu, A.; Murakami, N.; Sakakibara, J.; Tokuda, H.; Nishino, H.; Iwashima, A. Anti-Tumour-Promoting Glyceroglycolipids from the Green Alga, Chlorella Vulgaris. *Phytochemistry* **1995**, *40* (5), 1433–1437. https://doi.org/10.1016/0031-9422(95)00458-J.

(9) Justo, G. Z.; Silva, M. R.; Queiroz, M. L. S. Effects of the Green Algae Chlorella Vulgaris on the Response of the Host Hematopoietic System to Intraperitoneal Ehrlich Ascites Tumor Transplantation in Mice. *Immunopharmacology and Immunotoxicology* **2001**, *23* (1), 119–132. https://doi.org/10.1081/IPH-100102573.

(10) Shen, X.-F.; Liu, J.-J.; Chauhan, A. S.; Hu, H.; Ma, L.-L.; Lam, P. K. S.; Zeng, R. J. Combining Nitrogen Starvation with Sufficient Phosphorus Supply for Enhanced Biodiesel Productivity of Chlorella Vulgaris Fed on Acetate. *Algal Research* **2016**, *17*, 261–267. https://doi.org/10.1016/j.algal.2016.05.018.

(11) Shen, X.-F.; Qin, Q.-W.; Yan, S.-K.; Huang, J.-L.; Liu, K.; Zhou, S.-B. Biodiesel Production from Chlorella Vulgaris under Nitrogen Starvation in Autotrophic, Heterotrophic, and Mixotrophic Cultures. *J Appl Phycol* **2019**, *31* (3), 1589–1596. https://doi.org/10.1007/s10811-019-01765-1.

(12) Molina Grima, E.; Belarbi, E.-H.; Acién Fernández, F. G.; Robles Medina, A.; Chisti, Y. Recovery of Microalgal Biomass and Metabolites: Process Options and Economics. *Biotechnology Advances* **2003**, *20* (7), 491–515. https://doi.org/10.1016/S0734-9750(02)00050-2.

(13) Singh, G.; Patidar, S. K. Microalgae Harvesting Techniques: A Review. *Journal of Environmental Management* **2018**, *217*, 499–508. https://doi.org/10.1016/j.jenvman.2018.04.010.

(14) Lardon, L.; Hélias, A.; Sialve, B.; Steyer, J.-P.; Bernard, O. Life-Cycle Assessment of Biodiesel Production from Microalgae. *Environ. Sci. Technol.* **2009**, *43* (17), 6475–6481. https://doi.org/10.1021/es900705j.

(15) Shimako, A. H.; Tiruta-Barna, L.; Pigné, Y.; Benetto, E.; Navarrete Gutiérrez, T.; Guiraud, P.; Ahmadi, A. Environmental Assessment of Bioenergy Production from Microalgae Based Systems. *Journal of Cleaner Production* **2016**, *139*, 51–60. https://doi.org/10.1016/j.jclepro.2016.08.003.

(16) Kadir, W. N. A.; Lam, M. K.; Uemura, Y.; Lim, J. W.; Lee, K. T. Harvesting and Pre-Treatment of Microalgae Cultivated in Wastewater for Biodiesel Production: A Review. *Energy Conversion and Management* **2018**, *171*, 1416–1429. https://doi.org/10.1016/j.enconman.2018.06.074.

(17) Vandamme, D.; Foubert, I.; Muylaert, K. Flocculation as a Low-Cost Method for Harvesting Microalgae for Bulk Biomass Production. *Trends in Biotechnology* **2013**, *31* (4), 233–239. https://doi.org/10.1016/j.tibtech.2012.12.005.

(18) Vandamme, D.; Foubert, I.; Muylaert, K. Flocculation as a Low-Cost Method for Harvesting Microalgae for Bulk Biomass Production. *Trends in Biotechnology* **2013**, *31* (4), 233–239. https://doi.org/10.1016/j.tibtech.2012.12.005.

(19) Pugazhendhi, A.; Shobana, S.; Bakonyi, P.; Nemestóthy, N.; Xia, A.; Banu J, R.; Kumar, G. A Review on Chemical Mechanism of Microalgae Flocculation via Polymers. *Biotechnology Reports* **2019**, *21*, e00302. https://doi.org/10.1016/j.btre.2018.e00302.

(20) Renault, F.; Sancey, B.; Badot, P.-M.; Crini, G. Chitosan for Coagulation/Flocculation Processes – An Eco-Friendly Approach. *European Polymer Journal* **2009**, *45* (5), 1337–1348. https://doi.org/10.1016/j.eurpolymj.2008.12.027.

(21) Chen, G.; Zhao, L.; Qi, Y.; Cui, Y.-L. Chitosan and Its Derivatives Applied in Harvesting Microalgae for Biodiesel Production: An Outlook https://www.hindawi.com/journals/jnm/2014/217537/ (accessed Feb 3, 2020). https://doi.org/10.1155/2014/217537.

(22) Ahmad, A. L.; Mat Yasin, N. H.; Derek, C. J. C.; Lim, J. K. Optimization of Microalgae Coagulation Process Using Chitosan. *Chemical Engineering Journal* **2011**, *173* (3), 879–882. https://doi.org/10.1016/j.cej.2011.07.070.

(23) Ritthidej, G. C. Chapter 3 - Nasal Delivery of Peptides and Proteins with Chitosan and Related Mucoadhesive Polymers. In *Peptide and Protein Delivery*; Van Der Walle, C., Ed.; Academic Press: Boston, 2011; pp 47–68. https://doi.org/10.1016/B978-0-12-384935-9.10003-3.

(24) Bilanovic, D.; Shelef, G.; Sukenik, A. Flocculation of Microalgae with Cationic Polymers — Effects of Medium Salinity. *Biomass* **1988**, *17* (1), 65–76. https://doi.org/10.1016/0144-4565(88)90071-6.

(25) Rashid, N.; Rehman, S. U.; Han, J.-I. Rapid Harvesting of Freshwater Microalgae Using Chitosan. *Process Biochemistry* **2013**, *48* (7), 1107–1110. https://doi.org/10.1016/j.procbio.2013.04.018.

(26) Low, Y. J.; Lau, S. W. Effective Flocculation of Chlorella Vulgaris Using Chitosan with Zeta Potential Measurement. *IOP Conf. Ser.: Mater. Sci. Eng.* **2017**, *206*, 012073. https://doi.org/10.1088/1757-899X/206/1/012073.
(27) Matho, C.; Schwarzenberger, K.; Eckert, K.; Keshavarzi, B.; Walther, T.; Steingroewer, J.; Krujatz, F. Bio-Compatible Flotation of Chlorella Vulgaris: Study of Zeta Potential and Flotation Efficiency. *Algal Research* **2019**, *44*, 101705. https://doi.org/10.1016/j.algal.2019.101705.
(28) Garzon-Sanabria, A. J.; Ramirez-Caballero, S. S.; Moss, F. E. P.; Nikolov, Z. L. Effect of Algogenic Organic Matter (AOM) and Sodium Chloride on Nannochloropsis Salina Flocculation Efficiency. *Bioresource Technology* **2013**, *143*, 231–237. https://doi.org/10.1016/j.biortech.2013.05.125.
(29) Farid, M. S.; Shariati, A.; Badakhshan, A.; Anvaripour, B. Using Nano-Chitosan for Harvesting Microalga Nannochloropsis Sp. *Bioresource Technology* **2013**, *131*, 555–559. https://doi.org/10.1016/j.biortech.2013.01.058.
(30) Faridi, M. A.; Ramachandraiah, H.; Banerjee, I.; Ardabili, S.; Zelenin, S.; Russom, A. Elasto-Inertial Microfluidics for Bacteria Separation from Whole Blood for Sepsis Diagnostics. *Journal of Nanobiotechnology* **2017**, *15* (1). https://doi.org/10.1186/s12951-016-0235-4.
(31) Blockx, J.; Verfaillie, A.; Thielemans, W.; Muylaert, K. Unravelling the Mechanism of Chitosan-Driven Flocculation of Microalgae in Seawater as a Function of PH. *ACS Sustainable Chem. Eng.* **2018**, *6* (9), 11273–11279. https://doi.org/10.1021/acssuschemeng.7b04802.
(32) Cheng, Y.-S.; Zheng, Y.; Labavitch, J. M.; VanderGheynst, J. S. The Impact of Cell Wall Carbohydrate Composition on the Chitosan Flocculation of Chlorella. *Process Biochemistry* **2011**, *46* (10), 1927–1933. https://doi.org/10.1016/j.procbio.2011.06.021.
(33) Binnig, G.; Quate, C. F.; Gerber, C. Atomic Force Microscope. *Physical Review Letters* **1986**, *56* (9), 930–934.
(34) Formosa-Dague, C.; Gernigon, V.; Castelain, M.; Daboussi, F.; Guiraud, P. Towards a Better Understanding of the Flocculation/Flotation Mechanism of the Marine Microalgae Phaeodactylum Tricornutum under Increased PH Using Atomic Force Microscopy. *Algal Research* **2018**, *33*, 369–378. https://doi.org/10.1016/j.algal.2018.06.010.
(35) Besson, A.; Formosa-Dague, C.; Guiraud, P. Flocculation-Flotation Harvesting Mechanism of Dunaliella Salina: From Nanoscale Interpretation to Industrial Optimization. *Water Research* **2019**, *155*, 352–361. https://doi.org/10.1016/j.watres.2019.02.043.
(36) Vergnes, J. B.; Gernigon, V.; Guiraud, P.; Formosa-Dague, C. Bicarbonate Concentration Induces Production of Exopolysaccharides by Arthrospira Platensis That Mediate Bioflocculation and Enhance Flotation Harvesting Efficiency. *ACS Sustainable Chem. Eng.* **2019**, *7* (16), 13796–13804. https://doi.org/10.1021/acssuschemeng.9b01591.
(37) Blockx, J.; Verfaillie, A.; Eyley, S.; Deschaume, O.; Bartic, C.; Muylaert, K.; Thielemans, W. Cationic Cellulose Nanocrystals for Flocculation of Microalgae: Effect of Degree of Substitution and Crystallinity. *ACS Appl. Nano Mater.* **2019**, *2* (6), 3394–3403. https://doi.org/10.1021/acsanm.9b00315.
(38) Chen, L.; Chen, D.; Wu, C. A New Approach for the Flocculation Mechanism of Chitosan. *Journal of Polymers and the Environment* **2003**, *11* (3), 87–92. https://doi.org/10.1023/A:1024656813244.
(39) Demir, I.; Besson, A.; Guiraud, P.; Formosa-Dague, C. Towards a Better Understanding of Microalgae Natural Flocculation Mechanisms to Enhance Flotation Harvesting Efficiency. *Water Sci Technol* 2020. https://doi.org/10.2166/wst.2020.177.
(40) Verfaillie, A.; Blockx, J.; Praveenkumar, R.; Thielemans, W.; Muylaert, K. Harvesting of Marine Microalgae Using Cationic Cellulose Nanocrystals. *Carbohydrate Polymers* **2020**, *240*, 116165. https://doi.org/10.1016/j.carbpol.2020.116165.
(41) Alsteens, D.; Beaussart, A.; Derclaye, S.; El-Kirat-Chatel, S.; Park, H. R.; Lipke, P. N.; Dufrêne, Y. F. Single-Cell Force Spectroscopy of Als-Mediated Fungal Adhesion. *Anal. Methods* **2013**, *5* (15), 3657–3662. https://doi.org/10.1039/C3AY40473K.

(42) Yao, H.-B.; Fang, H.-Y.; Tan, Z.-H.; Wu, L.-H.; Yu, S.-H. Biologically Inspired, Strong, Transparent, and Functional Layered Organic–Inorganic Hybrid Films. *Angewandte Chemie International Edition* **2010**, *49* (12), 2140–2145. https://doi.org/10.1002/anie.200906920.
(43) Carapeto, A. P.; Ferraria, A. M.; Rego, A. M. B. do. Chitosan Thin Films on Glass and Silicon Substrates. *Microscopy and Microanalysis* **2015**, *21* (S5), 13–14. https://doi.org/10.1017/S1431927615013872.
(44) Formosa, C.; Grare, M.; Jauvert, E.; Coutable, A.; Regnouf-de-Vains, J. B.; Mourer, M.; Duval, R. E.; Dague, E. Nanoscale Analysis of the Effects of Antibiotics and CX1 on a Pseudomonas Aeruginosa Multidrug-Resistant Strain. *Sci. Rep.* **2012**, *2*. https://doi.org/10.1038/srep00575.
(45) Formosa-Dague, C.; Speziale, P.; Foster, T. J.; Geoghegan, J. A.; Dufrêne, Y. F. Zinc-Dependent Mechanical Properties of Staphylococcus Aureus Biofilm-Forming Surface Protein SasG. *PNAS* **2016**, *113* (2), 410–415. https://doi.org/10.1073/pnas.1519265113.
(46) Formosa-Dague, C.; Feuillie, C.; Beaussart, A.; Derclaye, S.; Kucharíková, S.; Lasa, I.; Van Dijck, P.; Dufrêne, Y. F. Sticky Matrix: Adhesion Mechanism of the Staphylococcal Polysaccharide Intercellular Adhesin. *ACS Nano* **2016**, *10* (3), 3443–3452. https://doi.org/10.1021/acsnano.5b07515.
(47) Higgins, M. J.; Molino, P.; Mulvaney, P.; Wetherbee, R. The Structure and Nanomechanical Properties of the Adhesive Mucilage That Mediates Diatom-Substratum Adhesion and Motility1. *Journal of Phycology* **2003**, *39* (6), 1181–1193. https://doi.org/10.1111/j.0022-3646.2003.03-027.x.
(48) Myllytie, P.; Salmi, J.; Laine, J. THE INFLUENCE OF PH ON THE ADSORPTION AND INTERACTION OF CHITOSAN WITH CELLULOSE. *BioResources* **2009**, *4* (4), 1647–1662.
(49) Simsek-Ege, F. A.; Bond, G. M.; Stringer, J. Polyelectrolyte Complex Formation between Alginate and Chitosan as a Function of PH. *Journal of Applied Polymer Science* **2003**, *88* (2), 346–351. https://doi.org/10.1002/app.11989.
(50) Barany, S.; Szepesszentgyörgyi, A. Flocculation of Cellular Suspensions by Polyelectrolytes. *Advances in Colloid and Interface Science* **2004**, *111* (1), 117–129. https://doi.org/10.1016/j.cis.2004.07.003.
(51) Boonsongrit, Y.; Mitrevej, A.; Mueller, B. W. Chitosan Drug Binding by Ionic Interaction. *European Journal of Pharmaceutics and Biopharmaceutics* **2006**, *62* (3), 267–274. https://doi.org/10.1016/j.ejpb.2005.09.002.
(52) Hertz, H. Ueber Die Beruhrung Fester Elastischer Korper. *Journal fur die reine und angewandte mathematik* **1881**, 156–171.
(53) Formosa, C.; Schiavone, M.; Martin-Yken, H.; François, J. M.; Duval, R. E.; Dague, E. Nanoscale Effects of Caspofungin against Two Yeast Species, Saccharomyces Cerevisiae and Candida Albicans. *Antimicrob. Agents Chemother.* **2013**, *57* (8), 3498–3506. https://doi.org/10.1128/AAC.00105-13.
(54) Guillard, R. R. L.; Lorenzen, C. J. Yellow-Green Algae with Chlorophyllide C2. *Journal of Phycology* **1972**, *8* (1), 10–14.
(55) Hutter, J. L.; Bechhoefer, J. Calibration of Atomic-Force Microscope Tips. *Review of Scientific Instruments* **1993**, *64* (7), 1868–1873.
(56) Francius, G.; Tesson, B.; Dague, E.; Martin-Jézéquel, V.; Dufrêne, Y. F. Nanostructure and Nanomechanics of Live Phaeodactylum Tricornutum Morphotypes. *Environ. Microbiol.* **2008**, *10* (5), 1344–1356. https://doi.org/10.1111/j.1462-2920.2007.01551.x.